ELSEVIER

Journal of Structural Geology 28 (2006) 1520–1535

JOURNAL OF STRUCTURAL GEOLOGY

www.elsevier.com/locate/jsg

The three-dimensional geometry and growth of forced folds above saucer-shaped igneous sills

Dorthe Møller Hansen*, Joe Cartwright

3DLab, School of Earth, Ocean and Planetary Sciences, Cardiff University, Main Building, Park Place, Cardiff CF10 3YE, Wales, UK

Received 15 June 2005; received in revised form 23 March 2006; accepted 4 April 2006
Available online 27 June 2006

Abstract

Forced folds formed at the seabed immediately overlying shallow (<1 km) saucer-shaped sills along the NE Atlantic Margin during the early Paleogene. Examples of this sill-fold relationship are exceptionally well imaged by high-resolution 3D seismic datasets from the NE Rockall Basin. The forced folds are domal in shape, 2–4 km in diameter, exhibit a structural relief of up to 350 m, and comprise sediment volumes of *ca.* 1 km^3. A comparison of the thickness distribution across and volume of a saucer-shaped sill with a high intrusion diameter to depth ratio and the structural relief and volume of its associated forced fold shows a remarkable equivalence. This has the important implication that the structural relief on intrusion-related forced folds can be used as an estimate of the thickness of the underlying sill. The analysed forced folds are interpreted to have formed through three continual growth stages that are directly linked to the mechanical emplacement of the underlying saucer-shaped sills. Their growth was associated with an increase in faulting of the overlying strata and influenced coeval or subsequent development of polygonal fault systems within the overburden. These structures represent a new type of four-way dip closed hydrocarbon trap.

Keywords: Forced fold; Saucer-shaped sills; 3D seismic; North Atlantic Igneous Province; NE Rockall Basin

1. Introduction

Forced folds were defined by Stearns (1978) as 'folds in which the final overall shape and trend are dominated by the shape of some forcing member below'. Vertical displacement of cover rocks and the development of forced folds above igneous intrusions has been described and inferred from field observations for almost a century (e.g. du Toit, 1920; Loewinson-Lessing, 1936; Tweto, 1951; Hotz, 1952). However, scale and two-dimensional limitations encountered at outcrop mean that this phenomenon has never been fully documented or resolved three-dimensionally. As a result, it remains unknown how the shape and volume of an igneous body is reflected in the geometry of an overlying forced fold. Resolving this issue has a number of important implications ranging from the mechanics of sill emplacement to forced fold evolution and hydrocarbon exploration.

Recently, extraordinarily well-defined forced folds have been observed overlying shallow-level igneous (Trude et al., 2003) and sandstone (Shoulders and Cartwright, 2004) intrusions imaged by 3D seismic data from along the NE Atlantic Margin. The recognition of intrusion-related forced folds on 3D seismic data opens up new avenues for the analysis of these structures in which the clear advantages offered by the three-dimensional properties available from 3D seismic datasets can be used to the full.

3D seismic interpretation of these recently recognised forced folds has already revealed a number of new insights. It has, for example, been demonstrated how seismic-stratigraphic correlation combined with biostratigraphic dating of onlap onto intrusion-related forced folds allows for the depth and timing of the underlying intrusion to be constrained

* Corresponding author. Present address: North Africa Research Group, School of Earth, Atmospheric and Environmental Sciences, University of Manchester, Williamson Building, Oxford Road, Manchester M13 9PL, UK. Tel.: +44 161 275 7679.
E-mail address: dorthe.hansen@manchester.ac.uk (D.M. Hansen).

0191-8141/$ - see front matter © 2006 Elsevier Ltd. All rights reserved.
doi:10.1016/j.jsg.2006.04.004

(Trude et al., 2003; Shoulders and Cartwright, 2004). This is of great importance in basin studies because: (1) it allows for the age of igneous intrusions, which are rarely encountered in wells, to be resolved independent of traditional radiometric dating; and (2) it offers the only available method for dating the timing of clastic intrusions. Previous studies have also shown how igneous intrusion-related forced folds influence depositional topography (Smallwood and Maresh, 2002; Trude et al., 2003) and thus potentially the distribution of hydrocarbon reservoir units. The forced folds themselves may form hydrocarbon traps and associated fracturing has important implications for basin fluid flow and hydrocarbon migration (Cosgrove and Ameen, 2000).

A number of detailed mechanical (Pollard and Johnson, 1973) and analogue models (Sanford, 1959; Stearns, 1978) have been developed in an attempt to explain the development of intrusion-related forced folds. Testing these models requires a three-dimensional understanding of the structural relief on the forced fold, their structural context, and the thickness distribution across the underlying sill and this information has not, until now, been available. In the NE Rockall Basin a number of forced folds developed above thick saucer-shaped sills are clearly imaged by 3D seismic data. These data offer a unique opportunity for the relationship between sill thickness and geometry and the geometry of an overlying forced fold to be constrained and hence for previous models for intrusion-related forced folding to be tested.

In this paper we provide, for the first time, a detailed analysis of the geometry of a forced fold developed above an exceptionally well-imaged, thick saucer-shaped sill. The structural relief and volume of the forced fold as well as the thickness and volume of the underlying saucer-shaped sill are constrained from 3D seismic data and compared in this analysis. The paper concludes by proposing a model for the growth of intrusion-related forced folds above shallowly emplaced saucer-shaped sills and outlining their implications.

2. Geological setting

This paper is based on the Tranche 38 (T38) 3D seismic dataset (subset of the PGS MC3D NRT-96/97/98 survey) acquired along the eastern flank of the NNE-SSW trending NE Rockall Basin (Fig. 1) north-west of the Outer Hebrides in a present-day water depth of 350–1300 m. The NE Rockall Basin forms the north-eastern part of the Rockall Trough and is bounded to the north by the Wyville-Thomson Ridge, to the east by the West Lewis Ridge and the Outer Hebrides platform and by the Geikie seamount and escarpment to the south (Waddams and Cordingley, 1999). The western margin is formed by the N-S trending Darwin-Geikie Ridge (Waddams and Cordingley, 1999). A Jurassic age for the NE Rockall Basin, similar to that of the Faeroe-Shetland Basin to the north-east, has been suggested for the basin as opposed to a Cretaceous origin for the Rockall Trough to the south-west (Waddams and Cordingley, 1999).

Seismic data (Tate et al., 1999) and gravity modelling (Waddams and Cordingley, 1999) suggest that more than 6000 m of Mesozoic section is present in the central part of the NE Rockall Basin. Data from exploration wells (e.g. 164/25-1ST and 164/25-2) show that Triassic, Jurassic, and Early Cretaceous sediments are present in the West Lewis Basin and West Lewis High areas suggesting that a similar range of sediments may be present in the NE Rockall Basin underneath the Tertiary succession (Tate et al., 1999). The post-rift succession is mainly comprised of basinal mudstones that contain some scattered basinal sands and slump units (Waddams and Cordingley, 1999). The Paleocene stratigraphy indicates that large-scale shallowing occurred during this time most likely due to regional thermal doming, whilst the Lower Eocene stratigraphy suggests a deepening probably in response to collapse of the thermal dome (Waddams and Cordingley, 1999). Mid-Tertiary episodes of inversion have affected the post-Lower Eocene stratigraphy and several inversion structures are found within the basin, e.g. the NW-SE trending Ymir Ridge (Tate et al., 1999; Waddams and Cordingley, 1999).

Extensive magmatic activity occurred in the NE Rockall Basin and North Rockall Trough from at least the latest Cretaceous until the Early Eocene (Tate et al., 1999). This resulted in the emplacement of large igneous centres (seamounts) in the axis of the Rockall Trough (e.g. Anton Dohrn, Rosemary Bank, and Darwin; Fig. 1) as well as smaller centres that sourced volcanoes and hypabyssal intrusions and extensive lava flows. The location of the igneous centres is likely to have been governed by intersecting NW-SE and ENE-WSW planes of structural weakness (Archer et al., 2005). The Anton Dohrn and Rosemary Bank igneous centres are thought to be Late Cretaceous in age, whilst the Darwin Centre, adjacent to the NE Rockall Basin, is likely to be slightly younger in age, yielding Paleocene dates (Tate et al., 1999). High amplitude reflections interpreted as lava flows and sills of early Tertiary age cover extensive areas of the basins (Figs. 1b and 2; Wood et al., 1988). The source of the lava flows is poorly constrained, but isochore maps indicate that the basalt interval thickens towards the Darwin Igneous Centre suggesting that the basalt may have emanated from there (Tate et al., 1999). Igneous sills are intruded into Mesozoic strata underlying the lava flows (Wood et al., 1988).

$^{40}Ar/^{39}Ar$ dating of igneous sills in the 164/7-1 exploration well located approximately 100 km north of the survey area has revealed some of the oldest ages in the North Atlantic indicating an Early Paleocene age (63–64 ± 0.5 My, Archer et al., 2005). A younger phase of intrusive activity has been documented in the nearby West Lewis Basin with dolerite sills encountered in well 164/25-1 yielding ages ~58–55 My (Archer et al., 2005). Recent dating of sill intrusion in the survey area based on the seismic-stratigraphic relationships of extrusive hydrothermal vents (Hansen, 2006) constrained the timing of intrusion in this area to approximately the Paleocene-Eocene transition (within the B–C interval described below). These independent observations suggest that there were several phases of intrusive magmatism in the NE Rockall Basin and the surrounding area during the Early Paleogene.

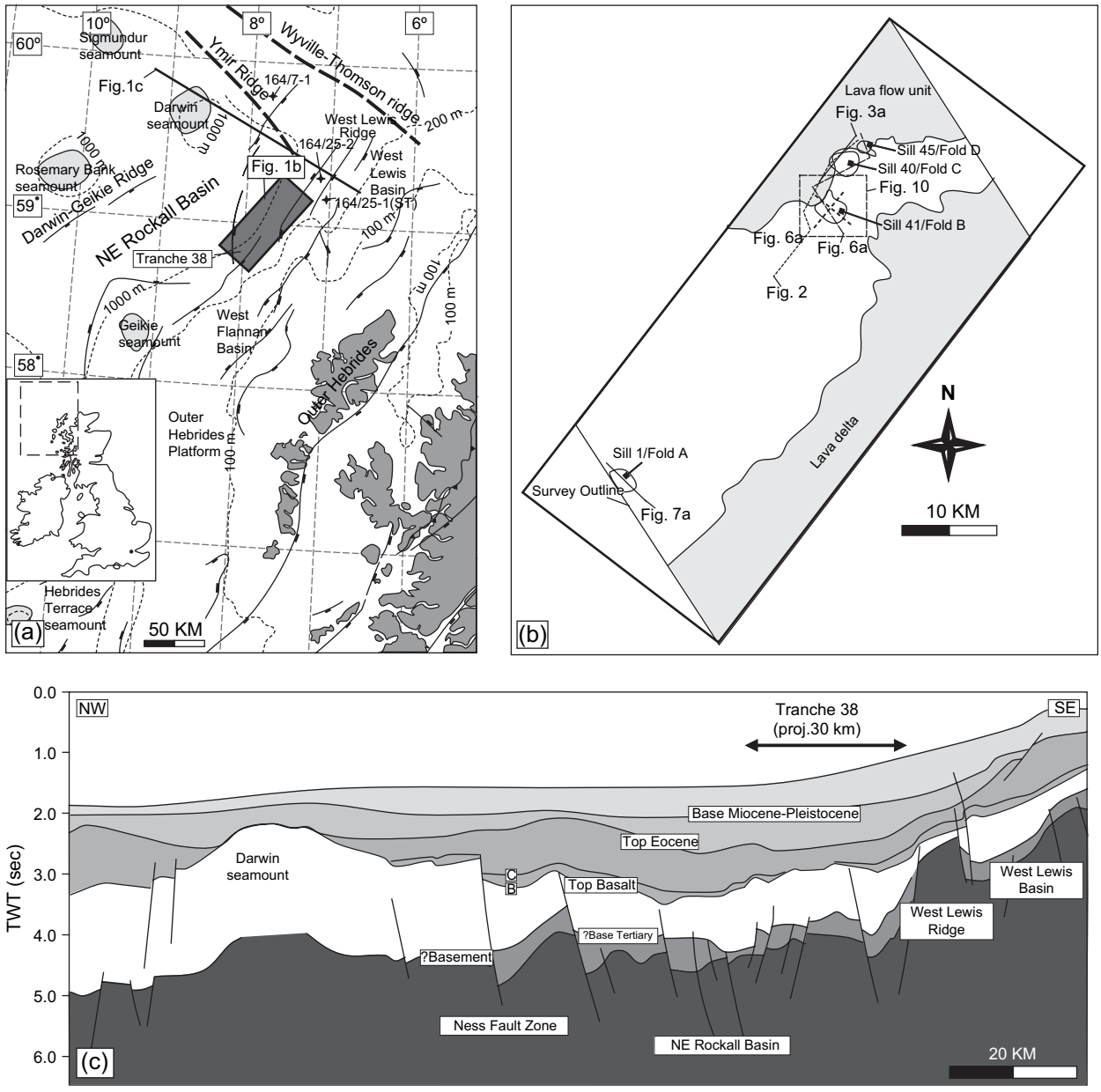

Fig. 1. Location and geological setting of study area. (a) Location map showing the location of the T38 3D seismic survey area in the NE Rockall Basin and exploration wells 164/7-1, 164/25-1(ST), and 164/25-2. (b) Schematic map showing the outline of the 3D seismic data, the distribution of the main extrusive units in the survey area, the locations of Sills 1, 40, 41, and 45, and seismic line locations. (c) Regional NW-SE trending section extending from the Darwin Igneous Complex to the NW to the West Lewis Basin to the SE. Note projected location of the T38 3D seismic survey area. See (a) for line location. Based on Tate et al. (1999).

3. Database

The T38 3D seismic dataset covers an area of 1400 km^2 and has a bin spacing in both the inline and crossline direction of 25 m. The data are zero-phase migrated and it is estimated that they exhibit a dominant frequency of approximately 35 Hz at the level where most intrusions are imaged. Assuming a sill velocity of 5.55 km/s (Skogly, 1998) this equates to a thickness of separability of approximately 80 m ($\lambda/2$, Sheriff and Geldart, 1995). This means that the top and base, and thus the thickness, of sills thinner than 80 m are not fully resolved by the data. However, local volume-based frequency extractions suggest that the frequency content surrounding some of the sills interpreted here is much lower, with average frequency spectra of 20–25 Hz, corresponding to $\lambda/2$ values of up to 135 m. Based on this it is considered likely that many sills thinner than 135 m will not be fully resolved.

Reasonable seismic velocities have been used to depth convert sill and sediment thicknesses. A velocity of 5.55 km/s $\pm$ 10% has been applied to the intruded magma (Skogly, 1998). A velocity of 2.5 km/s $\pm$ 20% has been applied to the host-rock in the shallower section (<2 s TWT below the present seabed).

3.1. Key seismic horizons

Four key seismic horizons (A–D) have been mapped in the survey area and tied to the nearby confidential exploration well 164/27-1 (Fig. 2). The horizons all dip towards the NW at <3°. Horizon A is close to Base Tertiary and has only been mapped locally. Horizon B marks the Top Faeroe Group of Late Paleocene age and it has been mapped across most of the survey area. Laterally Horizon B merges with a concordant package of high amplitude reflections imaged in the northern part of the survey area. This reflection package has been mapped across an area of 160 km^2 and is interpreted as a lava flow unit made up of a number of thin lava flows extruded onto the Top Faeroe Group (Horizon B) during the Late Paleocene. The lava flow unit extends beyond the survey boundary to the north and east. Horizon C has been mapped across most of the survey area. It marks the Top Balder Formation of earliest Eocene age (cf. Tate et al., 1999). The horizon is offset by faults spaced at 500–2000 m that form a polygonal fault pattern (e.g. Cartwright, 1994). The polygonal faults generally tip out downwards at Horizon B and terminate upwards a few tens of metres above Horizon C. The faults have dips of 40–45°, exhibit maximum throw values (D_{max}) of 150 m with displacement maxima located within the upper half of the B–C interval. Polygonal faults are believed to develop at very shallow burial depth (a few 100 m; Cartwright and Dewhurst, 1998). This suggests that the faults most likely developed in the Early Eocene, shortly after the deposition of Horizon C. A second tier of taller (up to 450 m) and more closely spaced (a few 100 m) polygonal faults is found above Horizon C, suggesting that a tier boundary is found slightly above Horizon C. The polygonal fault system recognised in the survey area is part of a wider polygonal fault system developed throughout the Rockall area (Cartwright and Dewhurst, 1998). A number of broad (2–4 km) domal folds with structural relief of up to 350 m are seen on time-structure maps of Horizon C. These folds are onlapped by the overlying strata. Horizon D has only been mapped in the western part of the survey area. It has a mounded morphology and both onlaps and downlaps onto Horizon C. This suggests that the C–D interval is of non-pelagic origin and that it was laid down through rapid deposition. The age of Horizon D is unknown, but based on the above interpretation of the C–D interval it is likely that it is Eocene in age.

4. 3D seismic interpretation of igneous sills in the T38 survey area

Complex networks of concordant and discordant, high amplitude, continuous reflections are imaged within the Cretaceous and Paleocene mud-dominated stratigraphy on seismic sections from sedimentary basins along the NE Atlantic Margin, including the NE Rockall Basin (Fig. 2). Well calibrations (e.g. exploration wells 164/25-1, 164/7-1, and 214/19-1) show that these high amplitude reflections represent igneous intrusions emplaced during the Paleocene and near the Paleocene-Eocene transition (Davies et al., 2002; Trude et al., 2003; Archer et al., 2005). Detailed 3D seismic mapping reveals that these sills exhibit a range of intrusive geometries and they commonly occur as saucer-shaped bodies imaged as smooth concave upward shapes on vertical seismic sections (Hansen et al., 2004; Thomson and Hutton, 2004). Individual saucer-shaped sills generally have diameters of <10 km, cover areas of a few tens of km^2, and exhibit a vertical relief of 500–800 m, however, occasionally cross-cutting >1500 m of stratigraphy (Hansen, 2004).

The sills mapped in the study area cover most of the survey area and span a vertical section >2 km with the shallowest sills terminating within the B–C interval. The general character and stratigraphic context of sills mapped in the study area

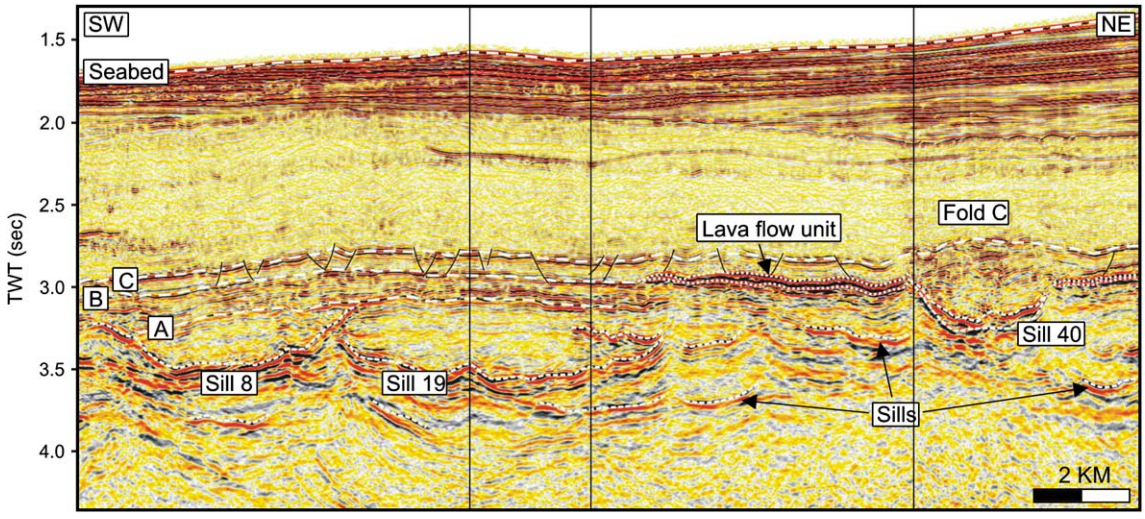

Fig. 2. SW-NE trending 3D seismic section through the T38 survey area illustrating main features described in the text. The section shows an interlinked network of igneous sills and the three mapped seismic horizons (A, B, and C). Sill 40 has a concave upward cross-sectional geometry and tips out at the level of Horizon B on to which a lava flow unit has been extruded. Above Sill 40 Fold C is developed. Horizon C is offset by faults that tip out downwards at Horizon B. The T38 3D seismic data are displayed using normal standard polarity (SEG standards; Sheriff, 2002) with black indicating maximum peak amplitude and red minimum peak amplitude. See Fig. 1b for line location.

is illustrated with reference to Fig. 2. Sill 8 has an upward concave geometry with a 3 km wide concordant basal section and edges that transgress discordant to stratigraphy at angles of <20° (present day). It exhibits a vertical relief of approximately 550 m. The north-eastern sill tip terminates at Horizon A, whilst the south-western tip transgresses across Horizon A and terminates within the A–B interval. The south-western tip of Sill 19 is linked to the north-eastern transgressive limb of Sill 8 through a Class B junction relationship (cf. Hansen et al., 2004). Class B sill-sill junctions are characterised by an abutment relationship between two sills. This type of junction is likely to form in densely intruded sequences where sills obstruct the propagation path of other sills. Class B junctions may also form as a result of bi-directional propagation away from a transgressive sill tip where planes of weakness or barriers to magma transport are encountered and therefore also represent sill-sill feeders (Hansen et al., 2004). Sill 19 is 3 km wide and exhibits a concave upward cross-sectional geometry with a vertical relief of almost 400 m. The north-eastern tip of Sill 19 terminates below Horizon A and appears to feed a number of smaller near-concordant sills. Sill 40 is seen to the NE. This sill is described in detail in a later section. Immediately above Sill 40 Horizon C exhibits a folded geometry (Fold C). This sill-fold relationship is a common feature above shallowly emplaced (<1 km below paleo-seabed) sills in the survey area and more generally along the NE Atlantic Margin and is the primary focus of this paper.

4.1. Detailed saucer-shaped sill geometries

Several saucer-shaped sills have been mapped in the T38 survey area and two of these (sills 40 and 41) that are particularly well imaged and exceptionally thick (>135 m), are described in detail below. Both sills exhibit a smoothly curved concave upward cross-sectional geometry and are clearly discordant with the surrounding host-strata. *Sill 40* (Figs. 2 and 3) measures 3.2 km by 2.7 km and covers an area of 6.5 km^2. It is intruded at a maximum depth of approximately 900 m below the contemporaneous seabed and has a maximum vertical relief of just over 400 m. It exhibits a clear change in thickness between the thick (~300 m) central basal part of the sill and the transgressive (25° present day) sill edge as seen in top and base reflections. Sill 40 has an estimated volume of *ca.* 1.1 km^3. *Sill 41* (Fig. 4) is very well imaged and both the top and base sill reflections are clearly identifiable over nearly the full extent of the sill. It measures 3 km by 2.5 km, covers an area of approximately 7.4 km^2, and comprises a magma volume of *ca.* 1 km^3. It is emplaced at a maximum depth of just less than 1 km below the paleo-seabed and has a vertical relief of approximately 300 m. The sill exhibits a clear decrease in thickness between the central basal part and the transgressive (16° present day) sill edge and exhibits a maximum thickness of approximately 300 m.

The thickness of sill 41 was measured in detail and depth converted along 6 cross-sectional transects across the sill and the data are shown in Fig. 5. The graphs show that the sill has a central thick region (200–300 m) and that the thickness decreases gradually towards the sill edge at gradients of approximately 0.3–0.4.

5. 3D seismic interpretation of folds at Top Balder Formation

5.1. General characteristics

One of the most remarkable observations made from the seismic data is the spatial coincidence between shallowly emplaced saucer-shaped sills (including sills 40 and 41) and folds at the Top Balder horizon (Horizon C). This relationship is shown in Fig. 6 where Horizon C is clearly folded

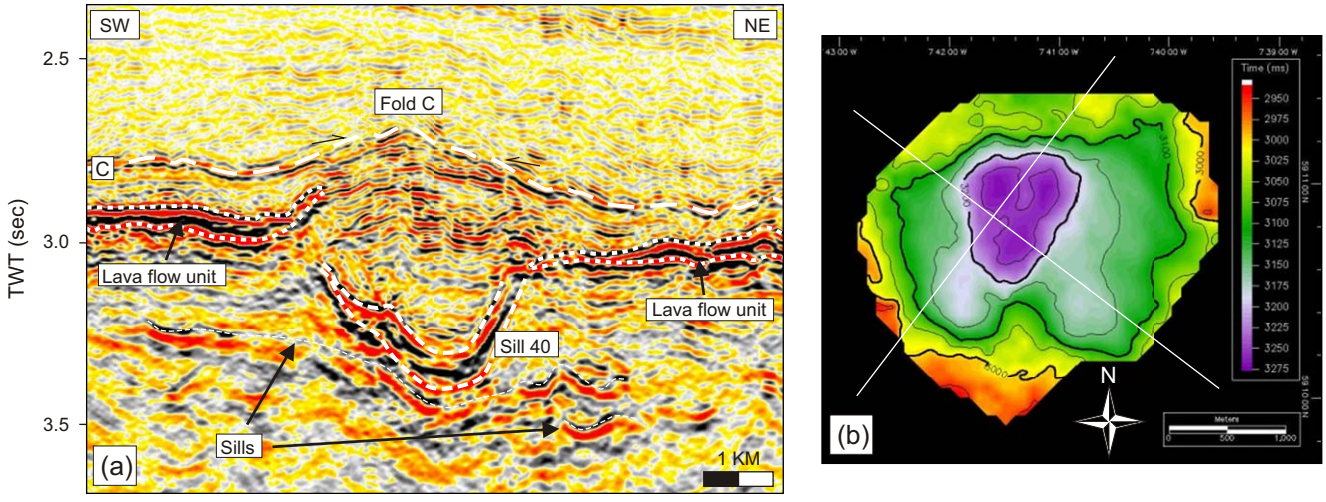

Fig. 3. (a) 3D seismic section illustrating the concave upward cross-sectional geometry of Sill 40. Note upward displacement of lava flow unit above SW transgressive limb of the sill and spatial coincidence with Fold C. See Fig. 1b for line location. (b) Time-structure map of Sill 40. Sill 40 is near-circular in planview, measures 3.2 km by 2.7 km, covers an area of 6.5 km^2, and has a maximum vertical relief of just over 400 m. It exhibits a clear change in thickness between the thick (~300 m) central basal part of the sill and the transgressive (25° present day) sill edge as seen in top and base reflections. Sill 40 comprises an estimated magma volume of *ca.* 1.1 km^3. Fig. 14 line locations are shown for reference.

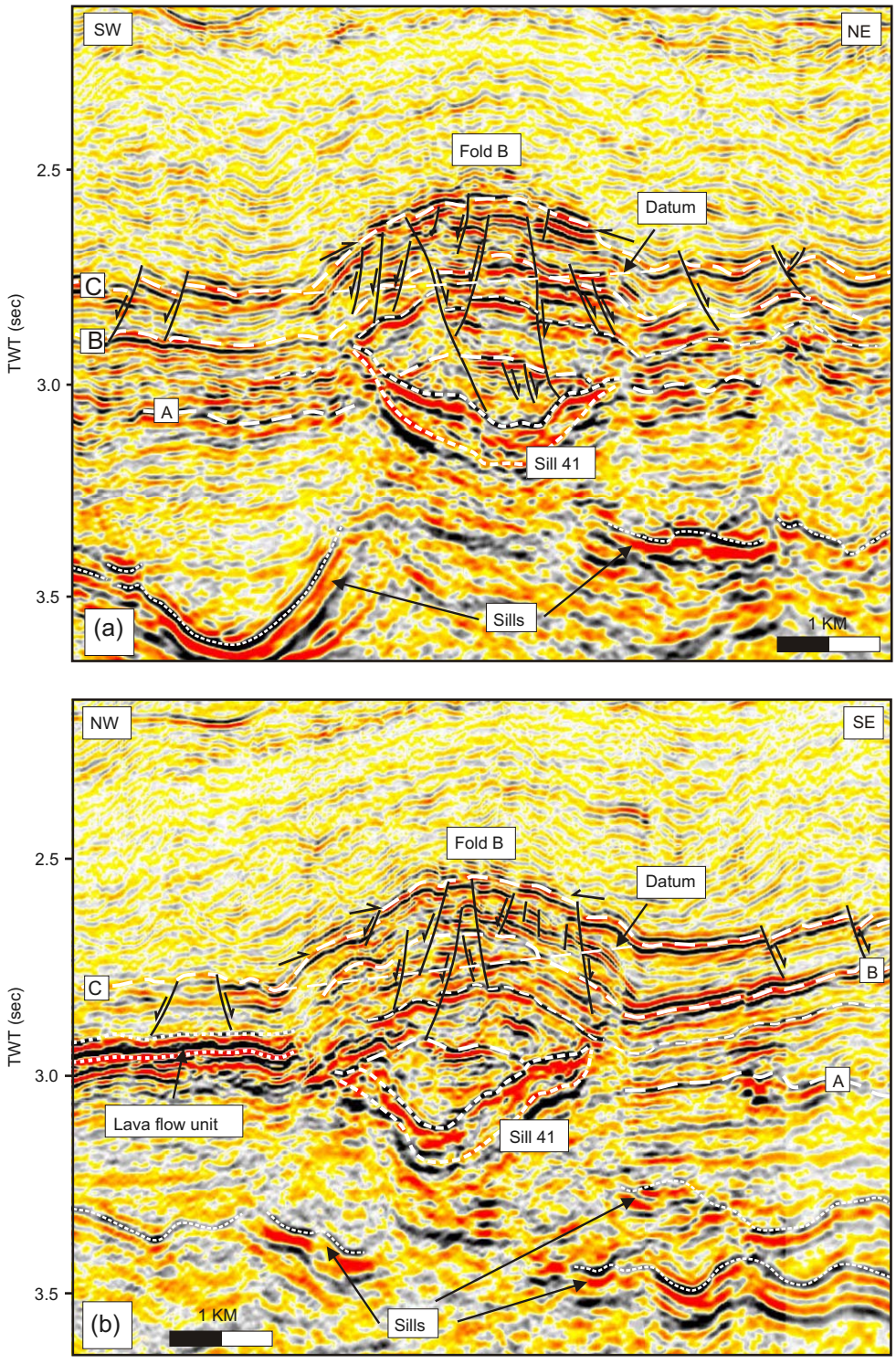

Fig. 4. 3D seismic sections illustrating the sill-fold relationship between Sill 41 and Fold B. Sill 41 is an exceptionally thick saucer-shaped sill that exhibits a characteristic concave upward cross-sectional geometry. It measures 3 km by 2.5 km, covers an area of approximately 7.4 km^2, has a vertical relief of approximately 300 m, and comprises a magma volume of *ca*. 1 km^3. The sill exhibits a clear decrease in thickness between the central basal part and the transgressive (16° present day) sill edge and exhibits a maximum thickness of approximately 300 m. Fold B is defined upwards by the continuous Horizon C, which is locally onlapped by overlying divergent stratal reflections. Note that the stratal reflections imaged between Sill 41 and Horizon B are more intensely faulted than the same interval away from the fold. Line locations are shown in Fig. 1b and correspond to b-b′ (a) and e-e′ (b) in Figs. 5 and 8.

immediately overlying three closely spaced sills (sills 40, 41, and 45). The folds have smooth domal cross-sectional geometries with flank dips of 10–15° and are onlapped by the overlying strata. This is illustrated with reference to Fold A located in the westernmost part of the survey area (Fig. 7). Fold A (Fig. 7a) has a near-circular domal planview geometry with a diameter of 4 km and a maximum structural relief of approximately 130 m. Fold A is located directly above sill 1

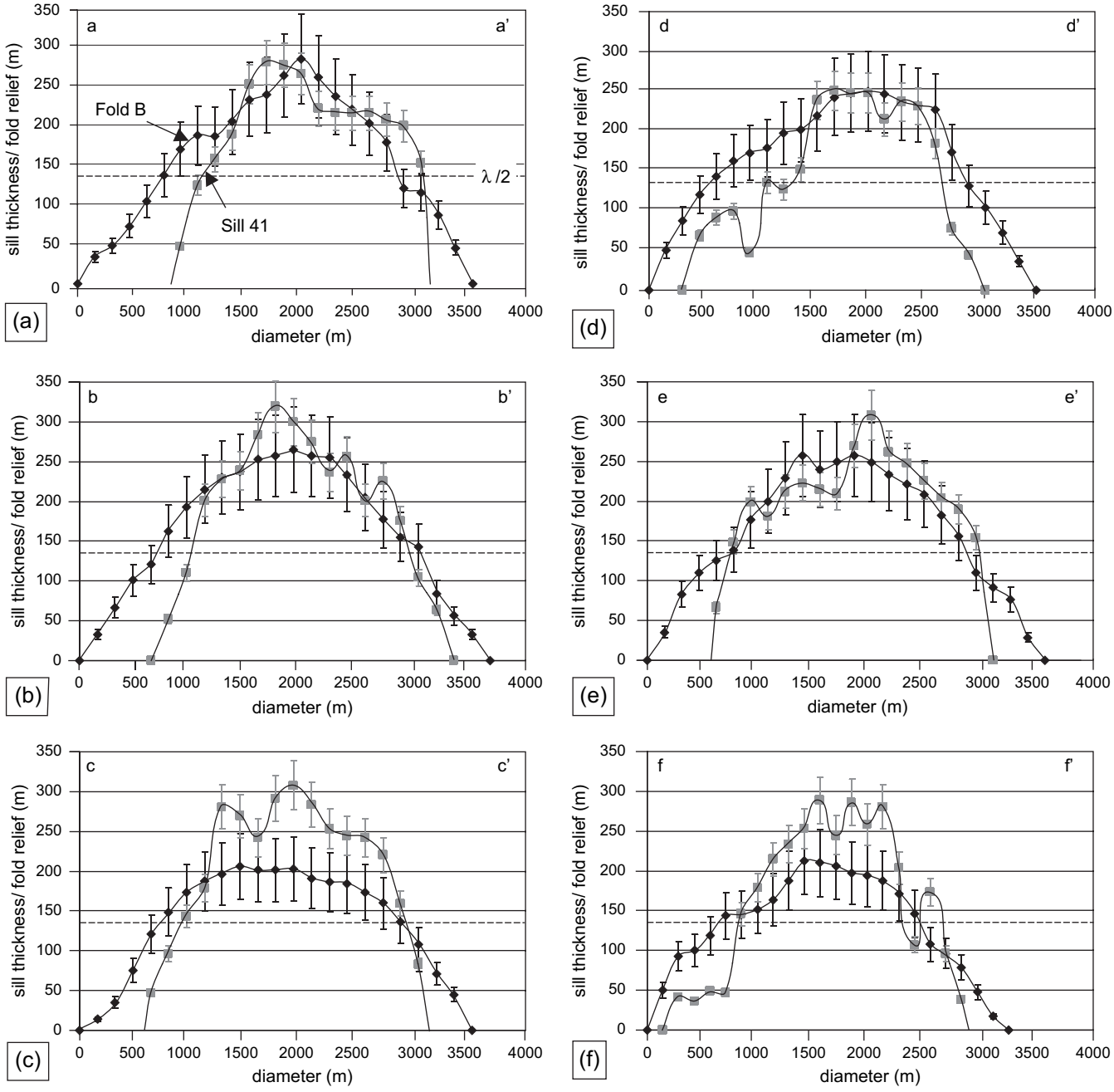

Fig. 5. The thickness of Sill 41 and the vertical relief on Fold B has been measured in detail and depth converted along 6 cross-sectional transects. The graphs show that Sill 41 has a central thick region (200–300 m) and that the thickness decreases gradually towards the sill edge at gradients of approximately 0.3–0.4. Fold B is gently arched, exhibits a maximum structural relief of approximately 250 m, has maximum flank dips of 12°, and exhibits an average outer arc strain of approximately 4.5%. From the graphs it is clear that the three-dimensional thickness distribution of Sill 41 is reflected in the structural relief on the overlying Fold B. The discrepancy seen towards the sill tip/fold margin is likely to be related to poor constraint on the sill thickness where this falls below the thickness of separability (λ/2). See Fig. 8 for line locations superimposed on isochore map of the structural relief on Fold B.

(Fig. 7b). The peripheries of both the fold and the sill are spatially coincident, and the crest of the fold is located vertically above the deepest part of the underlying sill. Sill 1 has a slightly elongated saucer-shaped geometry with the long axis oriented NW-SE, parallel to the predominant NW-SE magmatic emplacement trend recognised in the northern Rockall region (Archer et al., 2005). It measures 3.2 km by 2.2 km, covers an area of 4.5 km^2, and exhibits a vertical relief of approximately 400 m. Horizons A, B, and C have been deformed above the sill (Fig. 7a). Horizon A is cross-cut by the sill and the reflection segment that is nested within the concave shape of the sill is displaced upwards relative to the regional datum of the reflection segment seen outside the sill. Horizons B and C are both continuous across the sill, but exhibit folded geometries with fold limbs that coincide precisely in three dimensions with the sill tips. The C–D unit is significantly thinned across the crest of the fold and reflections within the unit clearly onlap Horizon C across the structure.

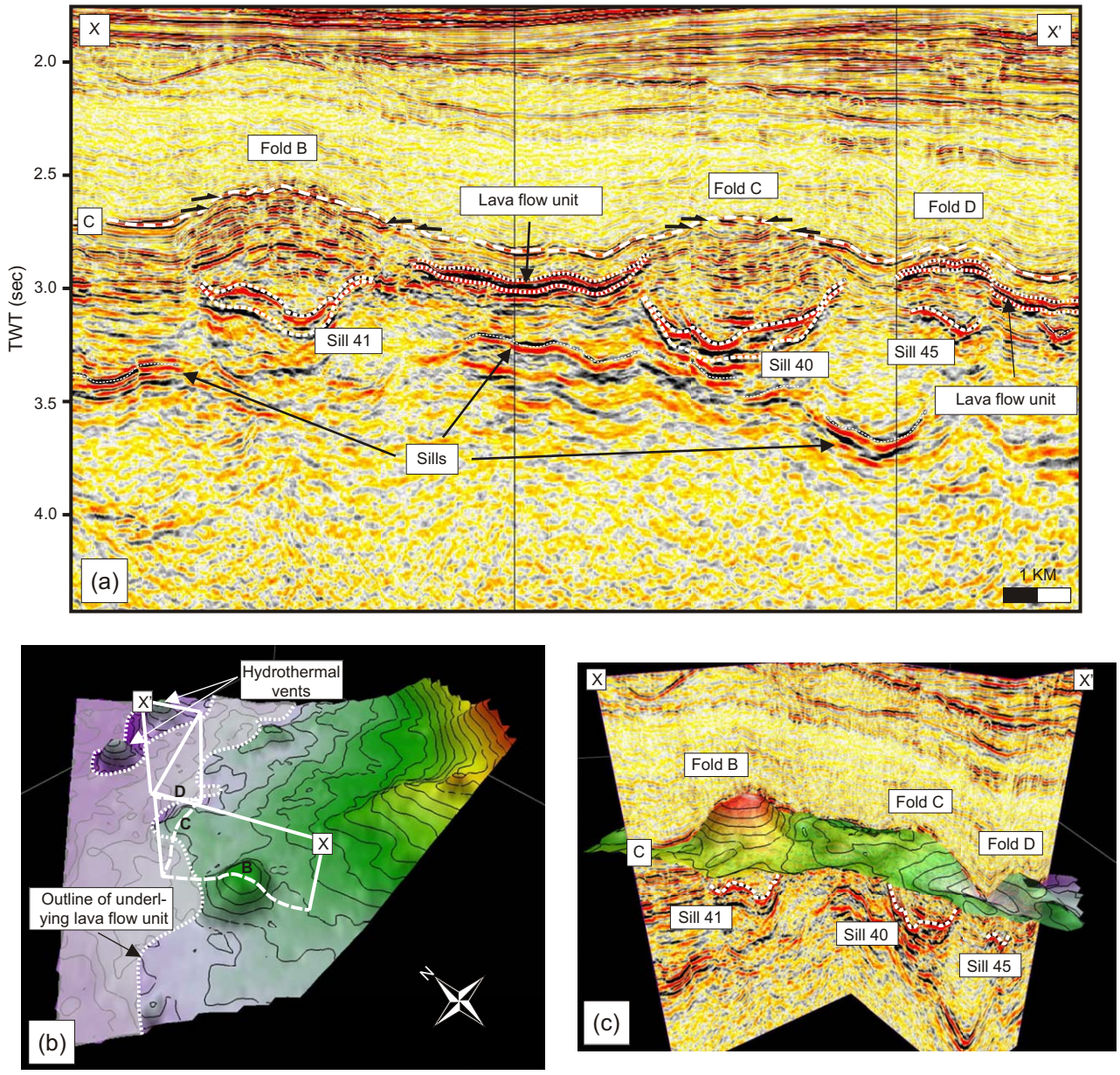

Fig. 6. Displays of seismic section and three-dimensional time-structure map of Horizon C, illustrating sill-fold relationships between Sill 41 and Fold B, Sill 40 and Fold C, and Sill 45 and Fold D. Note relationship with lava flow unit in (a) and (b), and location of hydrothermal vents in the northern part of the survey area. The time-structure maps displayed in (b) and (c) do not represent the full extent of Horizon C. See Fig. 1b for line location.

The clear spatial correspondence between saucer-shaped sills and folds at Horizon C strongly suggests a direct relationship between sill emplacement and fold development. Similar structures have recently been described from 3D seismic surveys in the Faeroe-Shetland Basin (Smallwood and Maresh, 2002; Trude et al., 2003). The structure described by Trude et al. (2003) measures approximately 2 km by 4 km and has a structural relief of around 280 m and is thus clearly comparable to in size to the structures described here. These structures were interpreted as forced folds formed at the paleo-seabed in order to accommodate the added thickness provided by the forcible intrusion of underlying igneous sills.

5.2. Detailed interpretation of the relationship between Sill 41 and Fold B

The largest domal fold is Fold B (Figs. 4, 6, and 8), which is located immediately above the well-imaged and thick Sill 41. Fold B is circular in planview, 3.5 km in diameter, covers an area of 13 km^2, and comprises an estimated sediment volume of 1.2 km^3. The fold is defined upwards by Horizon C, which is locally onlapped by overlying divergent stratal reflections (Fig. 4). The underlying Horizons A and B are also folded and exhibit a concordant relationship with Horizon C. The fold exhibits an upward-widening geometry. Horizon C is continuous across the structure and exhibits

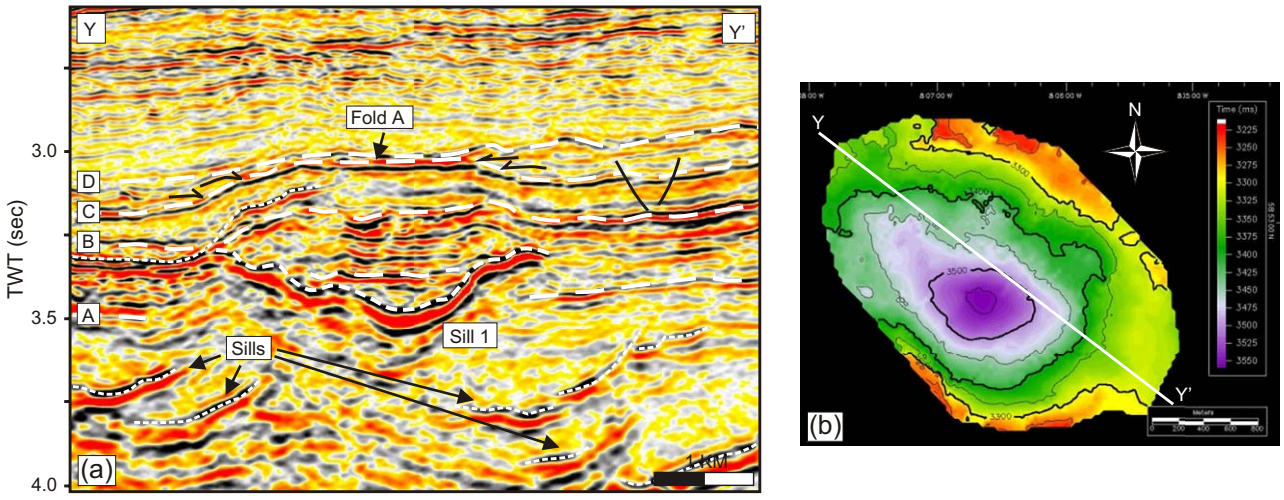

Fig. 7. (a) Vertical seismic section showing the cross-sectional geometry of Sill 1 and overlying Fold A. See Fig. 1b for line location. (b) Time-structure map of Sill 1. Sill 1 has a slightly elongated saucer-shaped geometry with the long axis oriented NW-SE. It measures 3.2 km by 2.2 km, covers an area of 4.5 km^2, and exhibits a vertical relief of approximately 400 m. Horizons A, B, and C have been deformed above the sill. Horizon A is cross-cut by the sill and the reflection segment that is nested within the concave shape of the sill is displaced upwards relative to the reflection segment seen outside the sill. Horizons B and C are both continuous across the sill, but exhibit folded geometries with fold limbs that coincide precisely in three dimensions with the sill tips. The C–D unit is significantly thinned across the crest of the fold and reflections within the unit clearly onlap Horizon C across the structure.

a maximum structural relief of approximately 250 m. This is illustrated by an isochore map of the depth-converted relief on Fold B as it is constrained by Horizon C and an interpolation of the datum of the fold relative to Horizon C (Fig. 8a). The shape and structural relief on Fold B is further quantified in a plot of the depth converted relief on the structure measured along 6 cross-sectional transects through the fold (Fig. 5). These graphs show that the fold is gently arched, has maximum flank dips of 12°, and exhibits an average outer arc strain of approximately 4.5%.

As with previous examples it is evident that Fold B is broadly coincident with the underlying Sill 41 and this spatial relationship is clearly demonstrated in Fig. 8b. The map shows that the structural relief on Fold B is greatest in the central part immediately overlying Sill 41 and that the domal fold structure extends approximately 500 m beyond the area covered by the sill in all directions. The relationship between the structural relief on Fold B and the thickness distribution across Sill 41 is also evident from the graphs shown in Fig. 5 from which it is clear that the three-dimensional thickness distribution of Sill 41 is reflected in the structural relief on the overlying Fold B. This is particularly evident across the central part of the sill where the sill thickness and structural relief on Fold B show a high level of equivalence. There is greater discrepancy at the sill tip-fold margin, which is likely to be partly a result of difficulties in constraining the true thickness of the sill as it falls below the thickness of separability. The relationship between sill thickness and structural relief on Fold B was further analysed by plotting the structural relief vs. sill thickness (Fig. 9). This graph shows a clear relationship between sill thickness and fold relief with a correlation value (R^2) of almost 60%.

5.3. Description and interpretation of Fold B fault pattern

The calculated 4.5% average arc strain across Fold B along the six depth-converted cross-sections is accommodated by a marked increase in the density of extensional faults within the A–C interval across the fold structure relative to away from the structure (Fig. 4). Planar to slightly listric normal faults are seen from the level of Sill 41 to Horizon C with maximum offsets of up to 100 m occurring at or slightly below Horizon B. The faults vary in height between <100 m–500 m showing a particularly marked increase in the number of short (<200 m) and tall (>400 m) faults compared to the area away from the fold (Fig. 4). The tallest faults are focused above the central part of the sill and exhibit the greatest D_{max} values. Horizon B is intensely faulted across Fold B with fault spacing down to as little as 200 m. This is in sharp contrast to the general lack of faulting of Horizon B away from the structure. The majority of faults dip away from the fold crest towards the edge of the fold structure with dip angles ranging between 25–50°. The fault pattern over and around Fold B is best seen on a time-dip attribute map of Horizon C (Fig. 10). The time-dip attribute highlights changes in dip of an interpreted seismic reflection and is, therefore, ideal for enhancing linear offsets of reflections as at fault contacts (Dalley et al., 1989; Hesthammer, 1998). A segmented concentric fault enclosing an area approximately 2 km in diameter dominates the area found within the outline of the sill (Fig. 10). A comparison with seismic profiles shows that the fault segments that link to form the concentric fault are normal, exhibit limited throws of a few tens of metres, and dip outwards away from the crest of the fold structure. In an area extending

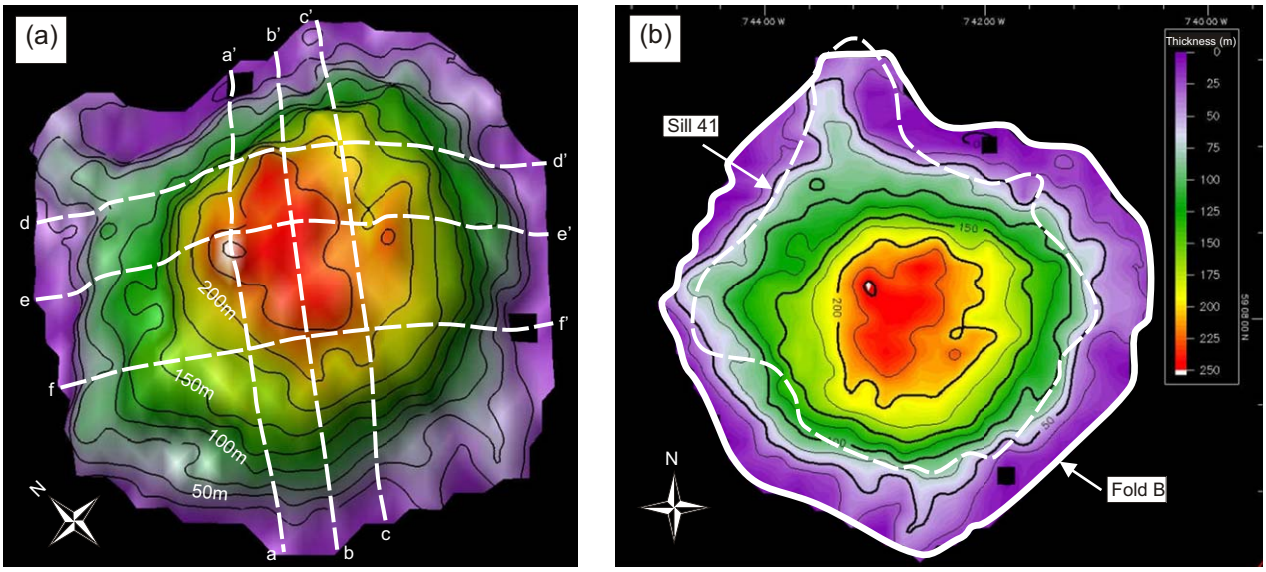

Fig. 8. (a) Isochore map of the depth-converted relief on Fold B as it is constrained by Horizon C and an interpolation of the datum (see Fig. 4) of the fold relative to Horizon C. The fold exhibits a maximum structural relief of approximately 250 m. Superimposed line locations refer to graphs shown in Fig. 5. (b) Fold B is spatially coincident with the underlying Sill 41. The structural relief on Fold B is greatest in the central part immediately overlying Sill 41.

approximately 2 km beyond the limit of the underlying sill the pattern is very different and characterised by radial faults that are orthogonal to the concentric fault and the outline of Sill 41. Beyond this area the faults exhibit a polygonal fault pattern.

A similar change in polygonal fault pattern has previously been observed above salt diapirs (Davison et al., 2000), mud diapirs (Hansen et al., 2005), and hydrothermal vents (Hansen, 2006). The re-organisation of polygonal faults above these structures occurs due to interference between the stress field linked to the growth of and differential compaction above the structures and the stress field within which polygonal faults form. This is important because it allows for the relative timing of folding and polygonal fault development to be constrained. The pattern indicates that the folding must have occurred either prior to or coeval with the development of the polygonal faults.

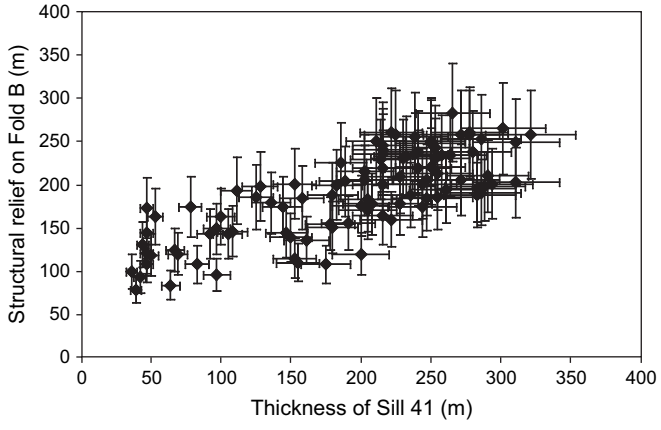

Fig. 9. X–Y plot ($n = 99$) showing linear relationship ($R^2 = 60\%$) between the thickness distribution across Sill 41 and the structural relief on the overlying Fold B. The graph shows good correlation (1:1) for larger values, but smaller values (<135 m) the sill thickness is consistently less than the relief on the structure. This discrepancy is likely to be related to poor constraint on the sill thickness where this falls below the thickness of separability (λ/2).

The increase in faulting seen across and around Fold B relative to away from the fold suggests that the majority of faults within the A–C interval across the fold are directly related to the folding process itself and unrelated to the polygonal fault system. Considering the sill-fold relationship, the fault pattern can be compared with mechanical and analogue models for deformation across laccoliths during their emplacement (Sanford, 1959; Pollard and Johnson, 1973; Stearns, 1978). This comparison is particularly appropriate because the measured thickness distribution across Sill 41 is comparable to that of many laccoliths (cf. Pollard and Johnson, 1973).

Sandbox experiments by Sanford (1959) and Stearns (1978) suggested that faults initially develop mainly above the periphery of the intrusion, with subsequent minor faulting affecting the sediments above the central part of the sill. The modelled fault pattern primarily differs from the seismic observations made here in displaying mostly reverse faults as opposed to the almost exclusive normal faulting seen across the fold structures in the survey area. This difference is most likely related to differences in material properties between the sandbox experiments and the much more cohesive mud-dominated folded lithology in the survey area, as the mud-dominated host-rock is much more prone to accommodating the fold-induced strain through soft-sediment deformation than the low cohesion sand used in the sandbox experiments.

Mechanical modelling by Pollard and Johnson (1973) suggested that deformation above growing laccoliths occurs mainly through bending and only once the intrusion has reached a lateral extent 2–4 times the depth of intrusion. The modelling indicated that both tensional and compressional bending strains develop in the host-rock above a growing laccolith with dominantly downward propagating fractures forming across the central part of the intrusion and upward

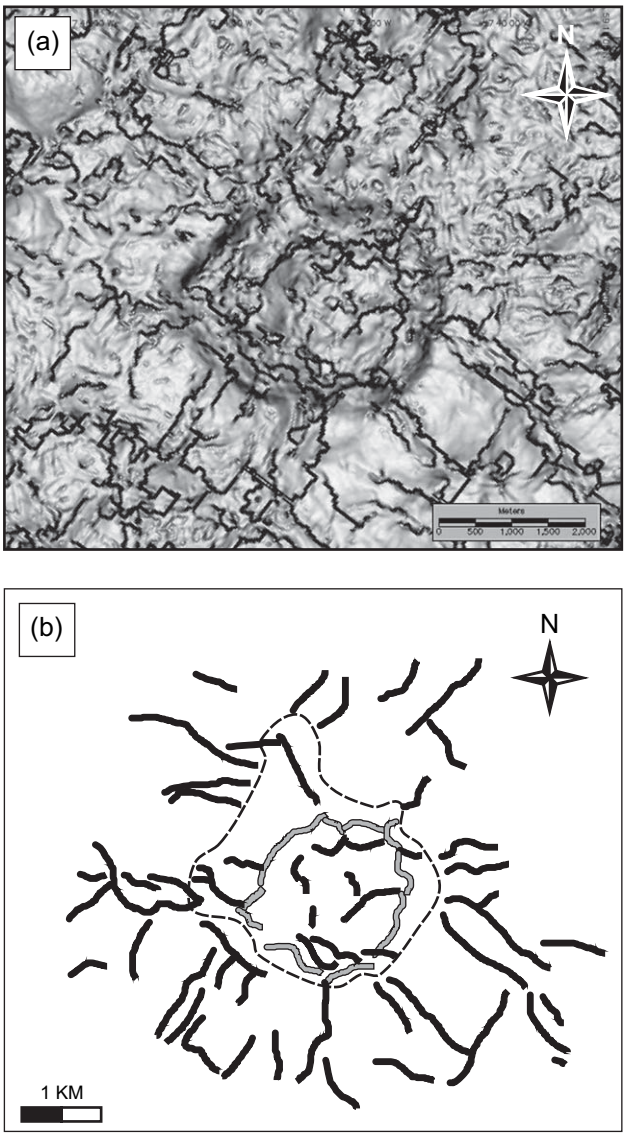

Fig. 10. Time-dip attribute map (a) and fault trace map (b) of Horizon C illustrating the fault pattern over and around Fold B. A segmented concentric fault (light grey shading) enclosing an area approximately 2 km in diameter dominates the area found within the outline of the underlying Sill 41 (dashed line). In an area extending approximately 2 km beyond the limit of Sill 41 the pattern is characterised by radial faults that are orthogonal to the concentric fault and the outline of Sill 41. Beyond this area the faults exhibit a polygonal fault pattern. The pattern indicates that the folding must have occurred either prior to or coeval with the development of the polygonal faults. See Fig. 1b for map location.

propagating fractures developing at the periphery of the intrusion. A peripheral dyke may form by subsequent infill of the peripheral fracture. Based on two-dimensional sections the distribution of faulting across Fold B is comparable to the modelling with the transgressive saucer edge representing a structural element equivalent to a peripheral dyke (cf. Pollard and Johnson, 1973; Cosgrove and Hillier, 2000). The tallest faults, which also exhibit the greatest D_{max} values, develop across the central part of the sill where greatest strain values are expected, and smaller faults forming in the intervening area where moderate strain is expected. The model does not explain the concentric normal fault seen above the central part of Sill 41 (Fig. 10). It most likely formed simply by outward collapse of the fold flanks (cf. McBirney, 1963; Lonsdale, 1983).

5.4. Constraining the timing of folding and sill intrusion

The timing of sill intrusion in the survey area is, by analogy with previous studies (cf. Trude et al., 2003; Shoulders and Cartwright, 2004), coeval with the folding if an intrusion-related forced fold origin applies to the sill-fold relationship. The timing of folding (Folds A–D) and hence the timing of sill intrusion (sills 1, 40, 41, and 45) has been constrained to the earliest Eocene using two independent methods based on seismic-stratigraphic relationships.

(1) Folds B, C, and D are located coincident with the southeastern periphery of the lava flow unit that extruded onto Horizon B in the northern part of the survey area during the Late Paleocene (Figs. 1b, 3 and 6a,b). From Fig. 3 it is evident that the edge of the lava flow unit is bent upwards above the southwestern tip of sill 40 maintaining a concordant relationship with the surrounding folded stratal reflections. Across sill 45 (Figs. 6a and 11) the tip of the lava flow unit has been detached from the main flow and clearly displaced upwards. These observations suggest that the lava flow unit was deformed by the folding process and thus indicate that folding post-dated the extrusion of the lava flow unit in the Late Paleocene.

(2) The timing of folding can be further and more precisely constrained by dating of onlap relationships onto the fold structures. Horizon C is onlapped by the overlying strata above Folds A–D (Figs. 3, 4, 6a, 7, and 11) suggesting that this horizon marks the timing of folding and that the folds were expressed at the sediment-water interface at the time of deformation. Seismic-stratigraphic correlation of Horizon C to exploration well 164/27-1 constrains the age of Horizon C and hence the timing of folding to the earliest Eocene. Lack of internal onlaps within the A–C interval indicates that folding occurred during one deformation event.

6. Discussion: The origin and growth of folds at Top Balder Formation

6.1. Origin of folds

Recently, the fold structures described here have been interpreted as shield volcanoes sourced from underlying ring feeders (Thomson, 2005). We disagree with this interpretation of folds A–D for a number of reasons: (1) stratal reflections can be mapped across the structures within the A–C interval (Figs. 4 and 7); (2) the high amplitude concave upward reflections seen underlying the structures (e.g. Fig. 6a) strongly resemble igneous sills mapped elsewhere (Hansen et al., 2004; Hansen, 2004) and are here interpreted as a saucer-shaped sills rather than chaotic basalts within ring faults as interpreted by Thomson (2004); and (3) the edge of the lava flow unit seen at

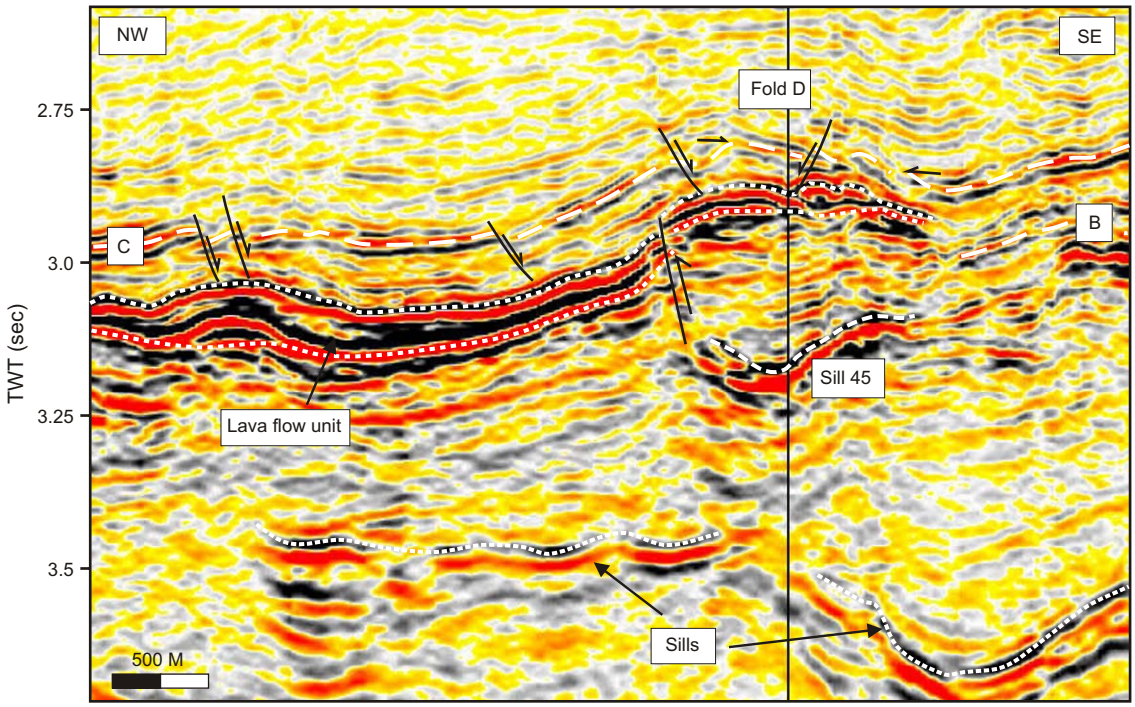

Fig. 11. Detachment and vertical displacement of the tip of the lava flow unit overlying Sill 45. The relationship indicates that intrusion of Sill 45 post-dates the timing of extrusion of the lava flow unit onto Horizon B during the Late Paleocene. Onlap onto Horizon C across Fold D suggests that Sill 45 was intruded in the earliest Eocene. See Fig. 1b for line location.

the level of Horizon B has been displaced upwards during the development of the structures following extrusion (Figs. 3 and 11).

The clear similarity in the geometry of individual fold structures developed at the Top Balder Formation boundary leads us to conclude that they share a common origin and that their spatial relationship with saucer-shaped sills indicates a causative relationship between the two. One possible interpretation of the sill-fold relationship is that the folds formed as a result of differential compaction above saucer-shaped sills (Fig. 12a). It has previously been suggested that the space for an intruding igneous sill is formed through fluid expulsion from the host rock surrounding the sill (Einsele et al., 1980). Subsequent differential compaction surrounding the sill would result in the development of a domal forced fold overlying the sill (Fig. 12a). However, a forced fold developed in this way would be associated with a divergent geometry of the stratal reflections within the overburden because of a more gradual evolution of fold amplitude during vertical loading under increased burial. Differential compaction cannot, therefore, be reconciled with the onlapping relationship seen onto Horizon C across the folds (e.g. Figs. 6 and 7).

We propose that these structures are forced folds formed due to vertical displacement above saucer-shaped sills during their emplacement (Fig. 12b). This interpretation is based on several lines of evidence: (1) the clear coincidence between the folds and well developed saucer-shaped sills (Fig. 6); (2) the clear displacement of the A–C interval overlying Sills 1 and 41 (Figs. 4 and 7) and upturning of the lava flow edge overlying Sills 40 and 45 (Figs. 3 and 11) strongly suggest upward vertical displacement of an existing sediment and lava pile overlying the sills; (3) the almost perfect correlation seen between the thickness and volume of Sill 41 and the structural relief and volume of Fold B (Fig. 5); and (4) the clear similarities between the structures mapped in the T38 survey area and similar structures mapped in the nearby Faeroe-Shetland Basin and interpreted as intrusion-related forced folds (Smallwood and Maresh, 2002; Trude et al., 2003).

Intrusion-related forced folds are widely described in the literature from outcrop (du Toit, 1920; Loewinson-Lessing, 1936; Tweto, 1951; Hotz, 1952), seismic (Smallwood and Maresh, 2002; Trude et al., 2003), mechanical (Pollard and Johnson, 1973; Pollard and Holzhausen, 1979), and analogue (Sanford, 1959; Stearns, 1978) studies. The proposed interpretation of the fold structures seen at the Top Balder Formation as intrusion-related forced folds can explain both the geometrical and structural relationships described in previous sections. This leads us to conclude that this is the only possible explanation for the structures described here.

6.2. Limited or lack of forced folding

This study has focused on four saucer-shaped sills intruded less than 1 km below the contemporaneous seabed and above which forced folds with structural relief >100 m are developed. Common to all of these sills is that they exhibit relatively large diameter-to-depth ratios (≥1.5).

In many cases stratal reflections overlying clearly imaged sills intruded at greater depth (>1 km) reveal no signs of internal discordance or onlap relationships (Fig. 2), suggesting that these sills intruded without causing any deformation of the water-sediment interface. Many of these sills exhibit

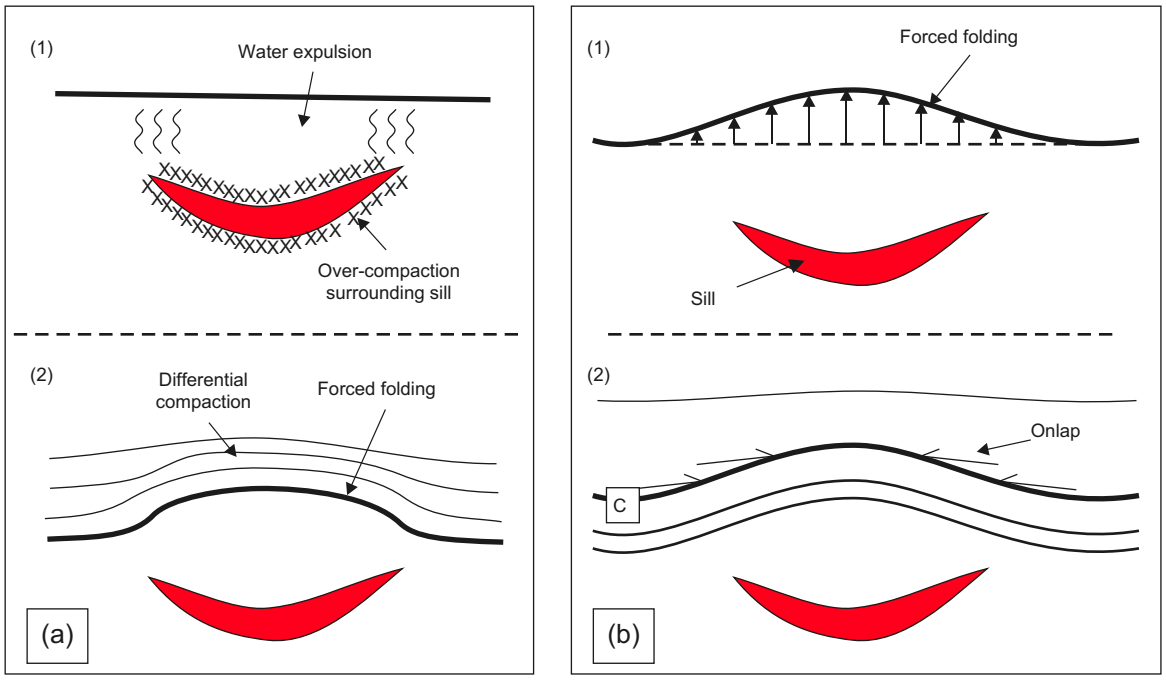

Fig. 12. Schematic illustrations of two ways in which intrusion-related forced folds may develop. (a) Differential compaction. (b) Upward displacement of overburden. The two mechanisms can be distinguished seismically through interpretation of the stratal reflection pattern in the overburden. The differential compaction mechanism (a) gives rise to a concordant relationship between the seabed at the time of intrusion and the overburden, whilst in the upward displacement mechanism (b) the seabed is deformed at the time of intrusion and onlapped by the overburden. Mechanism (b) is invoked for the sill-fold relationships described in this paper.

diameter-to-depth ratios of <1.5. The lack of forced folding above many of the deeper sills can be easily explained by invoking simple mechanical arguments. According to Pollard and Johnson (1973) and Fialko et al. (2001), the ratio of vertical displacement of overburden to sill thickness is governed by the ratio between sill diameter and intrusion depth. Sills that have a higher diameter-to-depth ratio will cause more bending of the overburden than sills that have a lower diameter-to-depth ratio. This means that intrusion of a sill with a given diameter at shallow depth will lead to greater upward displacement of the seabed than intrusion of a sill with the same diameter at greater depth. This relationship is further emphasised as ductile strain of overburden leads to upward-widening of the fold and vertical displacement decay away from the intrusion (cf. Pollard and Johnson, 1973; Withjack et al., 1990). Pollard and Johnson (1973) also found that a multi-layered host-rock offered less resistance to bending than a uniform host-rock because sliding of adjacent layers reduces the resistance to bending. It is highly plausible that these mechanical relationships play an important role in explaining why forced folding is only observed above a limited number of shallowly intruded sills that exhibit relatively large diameter-to-depth rations in the study area and not above the vast majority of the deeper sills.

However, even sills exhibiting a large diameter-to-depth ratio may in some cases have associated forced folds that have limited vertical relief compared to the thickness of the sill. In the case of Sill 41 the thickness of the saucer-shaped sill was fully translated to the overlying forced fold (Fold B; Fig. 5), whilst the thickness of Sill 40, which is emplaced at a similar depth and exhibits a similar diameter-to-depth ratio, is only partly recorded in the overlying Fold C (Fig. 13). This and other discrepancies elsewhere can be explained in a number of ways that invoke modification of the structural relief following fold development and mechanical constraints. These include: (1) the structural relief on the fold may have been modified by erosion or partial collapse prior to deposition of the overburden (cf. McBirney, 1963; Lonsdale, 1983). (2) Diagentic alteration within the folded sedimentary unit by hydrothermal fluids related to the intrusive process may result in anomalously high interval velocities (>2.5 km/s ± 20%). (3) The displacement of overburden above a sill may be masked by interference with displacement above surrounding sills.

6.3. Kinematic model for the growth of forced folds above saucer-shaped sills

The growth of forced folds above saucer-shaped sills is directly linked to the mechanical emplacement of the intrusive body. Based on the model of Pollard and Johnson (1973) and comparable models by Fialko (2001) and Malthe-Sørensen et al. (2004) the development of a saucer-shaped sill is a continuum process. In the following a simplistic kinematic model for the growth of a forced fold during the development of a saucer-shaped sill is proposed (Fig. 14). The model is illustrated with reference to three stages. The three stages need not be separate in time and are separated in the following only for illustrative purposes.

During the *first stage* of the model (Fig. 14a) there is limited deformation of the sediment-water interface above

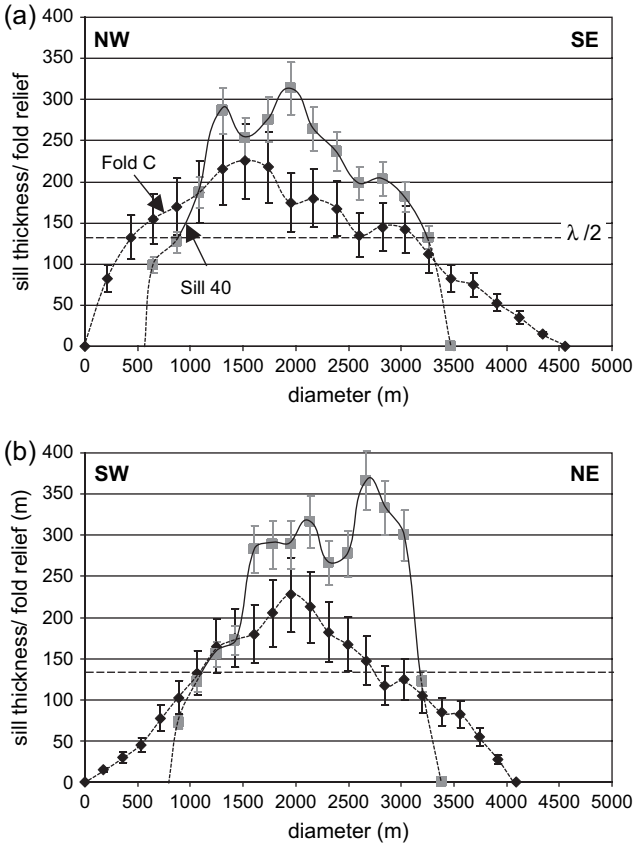

Fig. 13. Graphs showing the relationship between the thickness across Sill 40 and the structural relief on the overlying Fold C. Note that the sill is more than 100 m thicker in its central region than the structural relief across the crest of Fold C. This and similar discrepancies observed elsewhere can be explained in a number of ways that invoke modification of the structural relief following fold development as well as mechanical constraints. Please see text for further explanation. Line locations indicated in Fig. 3b.

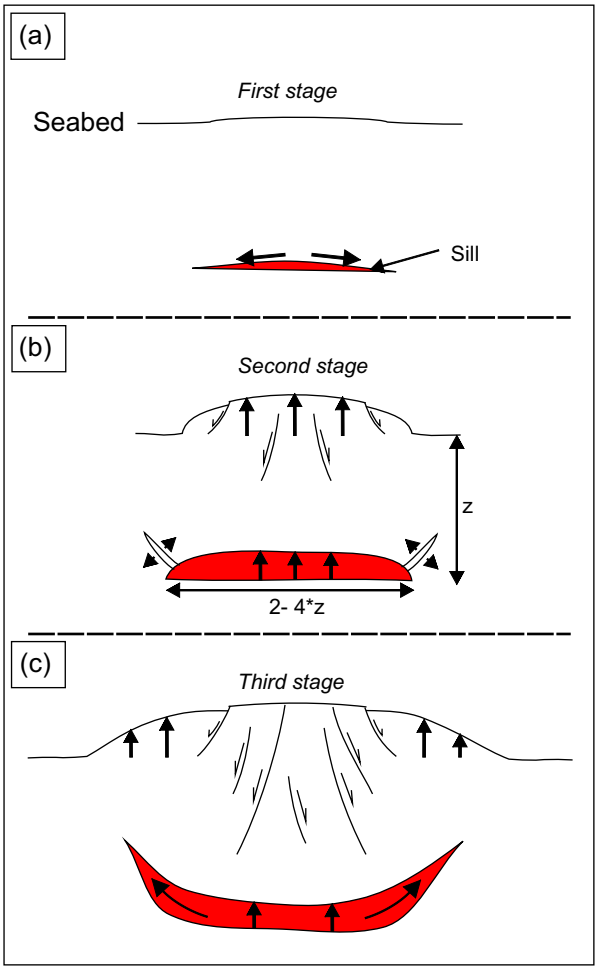

Fig. 14. Three-stage schematic kinematic model for the growth of a forced fold above saucer-shaped sills. Note that the three stages need not be separated in time and are separated here only for illustrative purposes. Please see text for description of kinematic model.

the newly initiated thin sill. After spreading over a distance of approximately 2 times the depth of intrusion the thickness of the sill starts to increase faster during the *second stage* (Fig. 14b). A forced fold with a structural relief equivalent to the thickness of the underlying sill is formed at the contemporaneous seabed. It exhibits steep flanks with fold limbs that are located immediately above the sill termination reflecting the thickness distribution across the underlying sill at this stage. Finally, towards the end of intrusion (*third stage*; Fig. 14c) the sill transgresses guided by peripheral fractures (peripheral dyke equivalent) and increased interaction with the free surface causing upward displacement along the periphery of the forced fold. The sill thins towards the tip and the tapering thickness profile is translated to the forced fold resulting in gently dipping fold limbs and the overall forced fold geometry seen on seismic sections.

7. Implications

7.1. Estimating the thickness of thin sills

One of the most important findings of this study is that their structural relief can be used to estimate the thickness distribution across the underlying sill where this is too thin for the upper and basal boundaries to be resolved by seismic data. The thickness estimate available using this method provides a minimum value of the true sill thickness. However, where the sill exhibits a high diameter-to-depth ratio the vertical relief of the overlying forced fold provides a very good estimate of the thickness of the underlying sill assuming the relief has not been significantly modified by external factors. This is important because it allows us to estimate intruded magma volumes more accurately, which in turn has implications for constraining the level of diagenetic alteration the host-rock has experienced. Conversely, however, sills exhibiting low diameter-to-depth ratios only cause limited or no vertical displacement of the overburden and this method of estimating sill thickness and hence magma volume is thus of limited use when dealing with sills of limited lateral extent intruded at depth.

7.2. The timing of intrusive events in the NE Rockall Basin

The seismic stratigraphic relationship of the intrusion-related forced folds provides a direct constraint on the timing

of sill intrusion independent of radiometric dating (Trude et al., 2003). Combining the findings of this and earlier studies it is clear that the T38 survey area has been affected by at least three magmatic events: (1) an early intrusive phase near the Paleocene-Eocene transition (within the B–C interval) was recently constrained from 3D seismic interpretation of hydrothermal vents developed in the northernmost corner of the survey area (Hansen, 2006). (2) A second intrusive phase during the earliest Eocene has been constrained in this paper from the onlapping relationship onto Horizon C (the Top Balder Formation) across the interpreted forced fold structures A–D (Figs. 6 and 7). (3) An extrusive magmatic event in the survey area that pre-dates the two intrusive events is evidenced by extrusion of a lava flow unit onto the Top Faeroe Group (Horizon B; Fig. 2) in the Late Paleocene.

In addition to the two intrusive episodes recognised in the survey area, recent $^{40}Ar/^{39}Ar$ dating of igneous sills in the 164/7-1 exploration well located approximately 100 km north of the survey area indicates an additional phase of intrusion in the NE Rockall in the Early Paleocene (Archer et al., 2005). This interpretation supports the recent suggestion that multiple discrete intrusive events took place along the NE Atlantic Margin during the Paleocene and Early Eocene (Hansen, 2006).

7.3. A new type of hydrocarbon trap

Forced folds above igneous sills represent a new type of hydrocarbon trap in the form of a four-way dip closure. If sandstone units are folded as part of the deformation process these structures have the potential to form hydrocarbon reservoirs that may subsequently be charged. There are, however, many unknowns surrounding these structures and their role in petroleum systems that will need to be better constrained as part of future work. These include: (1) to what extent has the folded and fractured sediments comprised within the forced fold structures been influenced by contact metamorphism and hydrothermal activity? (2) Are the gross rock volumes (unaffected by hydrothermal alteration) of these structures ever large enough to host significant hydrocarbon accumulations? (3) Is the best play potential related to these structures found in post-intrusion deep-water clastics that pinch-out against the folds rather than within the folded strata?

8. Conclusions

1. Forced (domal) folds exhibiting structural relief of up to $>$ 300 m and several kilometres in diameter formed at the sediment-water interface (Horizon C) in the earliest Eocene overlying a number of shallowly ($<$1 km) emplaced saucer-shaped sills in the T38 3D seismic survey area of the NE Rockall Basin in order to accommodate the added thickness provided by the forcible intrusion.

2. The geometry and structural relief on the forced folds reflects the thickness distribution of the underlying saucer-shaped sills. This has the important implication that the structural relief on the forced fold can be used to reconstruct the minimum thickness distribution across an underlying saucer-shaped sill in cases where these are too thin to be fully resolved by seismic data. In cases where a sill exhibits a large diameter-to-depth ratio ($\geq$1.5) the structural relief of the associated forced fold provides a very good estimate of the actual thickness of the underlying sill.

3. The development of forced folds leads to an increase in fault density within the folded stratigraphy and a re-organisation of any polygonal fault system that may form in the overburden coeval with or following folding.

4. Dating of sill intrusion in the study area based on seismic stratigraphic relationships of forced folds and hydrothermal vent structures reveals that sills were intruded during two discrete magmatic episodes near the Paleocene-Eocene transition and in the earliest Eocene.

5. Forced folds formed above saucer-shaped sills may form potential hydrocarbon traps. However, it remains unknown to what extent the folded stratigraphy is altered by hydrothermal fluids and contact metamorphism, which has significant implications for the quality of any reservoir that may be confined within such structures.

Acknowledgements

PhD sponsorships from Shell UK Exploration and Production and the Danish Research Agency (DMH) are greatly appreciated. Stuart Archer and Yuri Fialko are thanked for providing thorough and insightful reviews and Richard Lisle for providing useful comments. PGS Geophysical and the T38 licensing group (Statoil (UK) Ltd, Shell UK, and Mobil North Sea Ltd) are thanked for permission to publish images from the PGS MC3D NRT-96/97/98 3D seismic survey. Joanne Bagguley, Stephen Wright, and David Thomas (Shell) are thanked for their help during the course of this work. Schlumberger Geoquest is acknowledged for providing seismic interpretation software and technical support.

References

Archer, S.G., Bergman, S.C., Iliffe, J., Murphy, C.M., Thornton, M., 2005. Palaeogene igneous rocks reveal new insights into the geodynamic evolution and petroleum potential of the Rockall Trough, NE Atlantic Margin. Basin Research 17, 171–201.

Cartwright, J.A., 1994. Episodic basin-wide fluid expulsion from geopressured shale sequences in the North Sea Basin. Geology 22, 447–450.

Cartwright, J.A., Dewhurst, D., 1998. Layer-bound compaction faults in fine-grained sediments. Bulletin of the Geological Society of America 110, 1242–1257.

Cosgrove, J.W., Ameen, M.S., 2000. A comparison of the geometry, spatial organisation and fracture patterns associated with forced folds and buckle folds. In: Cosgrove, J.W., Ameen, M.S. (Eds.), Forced Folds and Fractures. Geological Society, 169. Special Publications, London, pp. 7–21.

Cosgrove, J.W., Hillier, R.D., 2000. Forced-fold development within Tertiary sediments of the Alba Field, UKCS: evidence of differential compaction and post-depositional sandstone remobilisation. In: Cosgrove, J.W., Ameen, M.S. (Eds.), Forced Folds and Fractures. Geological Society, 169. Special Publications, London, pp. 61–72.

Dalley, R.M., Gevers, E.C.A., Stampfli, G.M., Davies, D.J., Castaldi, C.N., Ruijtenberg, P.A., Vermeer, G.J.O., 1989. Dip and azimuth displays for 3D seismic interpretation. First Break 7, 86–95.

Davies, R., Bell, B.R., Cartwright, J.A., Shoulders, S., 2002. Three-dimensional seismic imaging of Paleogene dike-fed submarine volcanoes from the northeast Atlantic margin. Geology 30, 223–226.

Davison, I., Alsop, I., Birch, P., Elders, C., Evans, N., Nicholson, H., Rorison, P., Wade, D., Woodward, J., Young, M., 2000. Geometry and late-stage structural evolution of Central Graben salt diapers, North Sea. Marine and Petroleum Geology 17, 499–522.

du Toit, A.I., 1920. The Karoo dolerites. Transactions Geological Society of South Africa 33, 1–42.

Einsele, G., Gieskes, J.M., Curray, J., Moore, D.M., Aguayo, E., Aubry, M.-P., Fornari, D., Guerrero, J., Kastner, M., Kelts, K., Lyle, M., Matoba, Y., Molina-Cruz, A., Niemitz, J., Rueda, J., Saunders, A., Schrader, H., Simoneit, B., Vacquier, V., 1980. Intrusion of basaltic sills into highly porous sediments, and resulting hydrothermal activity. Nature 283, 441–445.

Fialko, Y., 2001. On origin of near-axis volcanism and faulting at fast spreading mid-ocean ridges. Earth and Planetary Science Letters 190, 31–39.

Fialko, Y., Khazan, Y., Simons, M., 2001. Deformation due to a pressurized horizontal circular crack in an elastic half-space, with applications to volcano geodesy. Geophysical Journal International 146, 181–190.

Hansen, D.M., 2004. 3D seismic characterisation of igneous sill complexes in sedimentary basins: North-East Atlantic Margin. Ph.D. Thesis, Cardiff University of Wales.

Hansen, D.M., 2006. The morphology of intrusion-related vent structures and their implications for constraining the timing of intrusive events along the NE Atlantic Margin. Journal of the Geological Society, London. 163, in press.

Hansen, D.M., Cartwright, J.A., Thomas, D., 2004. 3D seismic analysis of the geometry of igneous sills and sill junction relationships. In: Davies, R.J., Cartwright, J.A., Stewart, S.A., Lappin, M., Underhill, J.R. (Eds.), 3D Seismic Technology: Application to the Exploration of Sedimentary Basins. Geological Society, London, pp. 199–208. Memoirs 29.

Hansen, J.P.V., Cartwright, J.A., Huuse, M., Clausen, O.R., 2005. 3D seismic expression of fluid migration and mud remobilisation on the Gjallar Ridge, offshore mid-Norway. Basin Research 17, 123–140.

Hesthammer, J., 1998. Evaluation of the timedip, correlation and coherence maps for structural interpretation of seismic data. First Break 16, 151–167.

Hotz, P.E., 1952. Form of diabase sheets in south eastern Pennsylvania. American Journal of Science 250, 375–388.

Loewinson-Lessing, F., 1936. A contributions to the mechanics of intrusions. XVI International Geological Congress Report, 333–352.

Lonsdale, P., 1983. Laccoliths (?) and small volcanoes on the flank of the East Pacific Rise. Geology 11, 706–709.

Malthe-Sørensen, A., Planke, S., Svensen, H., Jamtveit, B., 2004. Formation of saucer-shaped sills. Geological Society. Special Publication 234, London. 215–227.

McBirney, A.R., 1963. Factors governing the nature of submarine volcanism. Bulletin of Volcanology 26, 455–469.

Pollard, D.D., Holzhausen, G., 1979. On the mechanical interaction between a fluid-filled fracture and the earth's surface. Tectonophysics 53, 27–57.

Pollard, D.D., Johnson, A.M., 1973. Mechanics of growth of some laccolithic intrusions in the Henry Mountains, 18. Bending and failure of overburden layers and sill formation. Tectonophysics, Utah, II. 311–354.

Sanford, A.R., 1959. Analytical and experimental study of simple geologic structures. Bulletin of the Geological Society of America 70, 19–52.

Sheriff, R.E., 2002. Encyclopedic Dictionary of Applied Geophysics. Society of Exploration Geophysicists, Tulsa, Oklahoma, U.S.A.

Sheriff, R.E., Geldart, L.P., 1995. Exploration Seismology. Cambridge University Press.

Shoulders, S.J., Cartwright, J., 2004. Constraining the depth and timing of large-scale conical sandstone intrusions. Geology 32, 661–664.

Skogly, O., 1998. Seismic characterization and emplacement of intrusives in the Vøring Basin. M.Sc. thesis, University of Oslo.

Smallwood, J.R., Maresh, J., 2002. The properties, morphology and distribution of igneous sills: modelling, borehole data and 3D seismic from the Faroe-Shetland area. In: Jolley, D.W., Bell, B.R. (Eds.), The North Atlantic Igneous Province: Stratigraphy, Tectonic, Volcanic and Magmatic Processes. Geological Society. Special Publication 197, London, pp. 271–306.

Stearns, D.W., 1978. Faulting and forced folding in the Rocky Mountains foreland. Geological Society of America Memoir 151, 1–38.

Tate, M.P., Dodd, C.D., Grant, N.T., 1999. The Northeast Rockall Basin and its significance in the evolution of the Rockall-Faeroes/East Greenland rift system. In: Fleet, A.J., Boldy, S.A.R. (Eds.), Petroleum Geology of Northwest Europe: Proceedings of the 5th Conference. Geological Society, London, pp. 391–406.

Thomson, K., 2004. Volcanic features of the North Rockall Trough: application of visualisation technique on 3D seismic reflection data. Bulletin of Volcanology 67, 116–128.

Thomson, K., 2005. Extrusive and intrusive magmatism in the North Rockall Trough. In: Doré, A.G., Vining, B. (Eds.), Petroleum Geology: Northwest Europe and Global Perspectives – Proceedings of the 6th Conference. Geological Society, London, pp. 1621–1630.

Thomson, K., Hutton, D., 2004. Geometry and growth of sill complexes: insights using 3D seismic from the North Rockall Trough. Bulletin of Volcanology 66, 364–375.

Trude, K.J., Cartwright, J.A., Davies, R.J., Smallwood, J.R., 2003. A new technique for dating igneous sills. Geology 31, 813–816.

Tweto, O., 1951. Form and structure of sills near Pando, Colorado. Geological Society of America Bulletin 62, 507–532.

Waddams, P., Cordingley, T., 1999. The regional geology and exploration potential of the NE Rockall Basin. In: Fleet, A.J., Boldy, S.A.R. (Eds.), Petroleum Geology of Northwest Europe: Proceedings of the 5th Conference. Geological Society, London, pp. 379–390.

Withjack, M.O., Olson, J., Peterson, E., 1990. Experimental models of extensional forced folds. American Association of Petroleum Geologists Bulletin 74, 1038–1054.

Wood, M.V., Hall, J., Doody, J.J., 1988. Distribution of early Tertiary lavas in the NE Rockall Trough. In: Morton, A.C., Parson, L.M. (Eds.), Early Tertiary Volcanism and the Opening of the NE Atlantic, Geological Society. Special Publication 39, London, pp. 283–292.